# Spray Coating Experiments: Setups and Methodologies


**The latest eBook from Advanced Optical Metrology. Download for free.**

*Spray Coating Experiments: Setups and Methodologies*, is the third in our Thin Films eBook series. This publication provides an introduction to spray coating, three article digests from Wiley Online Library and the latest news about Evident's Image of the Year Award 2022.

Wiley in collaboration with Evident, are committed to bridging the gap between fundamental research and industrial applications in the field of optical metrology. We strive to do this by collecting and organizing existing information, making it more accessible and useful for researchers and practitioners alike.

EVIDENT
OLYMPUS

WILEY

ADVANCED FUNCTIONAL MATERIALS
www.afm-journal.de



# A New Class of Organic Crystals with Extremely Large Hyperpolarizability: Efficient THz Wave Generation with Wide Flat-Spectral-Band

*Seung-Jun Kim, In Cheol Yu, Dong-Joo Kim, Mojca Jazbinsek, Woojin Yoon, Hoseop Yun, Dongwook Kim, Fabian Rotermund,* and O-Pil Kwon**

**In organic π-conjugated crystals, enhancing molecular optical nonlinearity of chromophores (e.g., first hyperpolarizability $\beta \geq 300 \times 10^{-30}$ esu) in most cases unfortunately results in zero macroscopic optical nonlinearity, which is a bottleneck in organic nonlinear optics. In this study, a new class of nonlinear optical organic crystals introducing a chromophore possessing an extremely large first hyperpolarizability is reported. With newly designed 4-(4-(4-(hydroxymethyl)piperidin-1-yl)styryl)-1-(pyrimidin-2-yl)pyridin-1-ium (PMPR) chromophore, incorporating a head-to-tail cation-anion O—H···O hydrogen-bonding synthon and an optimal selection of molecular anion into crystals results in extremely large macroscopic optical nonlinearity with effective first hyperpolarizability $\beta_{iii}^{eff}$ of $335 \times 10^{-30}$ esu. This is in sharp contrast to zero $\beta_{iii}^{eff}$ value for previously reported analogous crystals. An ultrathin PMPR crystal with a thickness of ≈10 µm exhibits excellent terahertz (THz) wave generation performance. Both i) broadband THz wave generation with a wide flat-spectral-band in the range of 0.7–3.4 THz defined at −3 dB and high upper cut-off generation frequency of > 7 THz as well as ii) high-generation efficiency (5 times higher THz amplitude than ZnTe crystal with a mm-scale thickness) are simultaneously achieved. Therefore, new PMPR crystals are highly promising materials for diverse applications in nonlinear optics and THz photonics.**

## 1. Introduction

Nonlinear optical materials are highly attractive for diverse applications in telecommunications, integrated optics, THz wave photonics, frequency conversion, and electro-optic modulation.[1–9] A large macroscopic second-order optical nonlinearity in materials is the key parameter to achieve efficient performance in these applications. In integrated photonic devices, large macroscopic second-order optical nonlinearity allows a low operation voltage (e.g., half-wave voltage in Mach–Zehnder interferometer that is reciprocally proportional to the electro-optic coefficient).[2–4] Also for THz photonic devices, the macroscopic optical nonlinearity is a crucial material parameter. For THz wave generators based on difference frequency generation (DFG) or optical rectification (OR), THz generation efficiency is proportional to the square of the second-order nonlinear optical susceptibility $\chi^{(2)}$,[9,10] while the detection sensitivity is proportional to the electro-optic coefficient for THz detection based on optical phase detection with electro-optic sampling (EOS) or THz-induced lensing methods.[9,11,12]

To obtain a large macroscopic optical nonlinearity in organic crystals, highly dipolar π-conjugated chromophores have to be self-assembled with a high-order parameter, optimally perfectly parallel, without inversion symmetry.[1,13,14] Unfortunately, introducing chromophores having an extremely large, top-level molecular optical nonlinearity (e.g., first hyperpolarizability $\beta \geq 300 \times 10^{-30}$ esu) into crystals mostly results in centrosymmetric self-assembly of chromophores, i.e., with inversion symmetry, which leads

S.-J. Kim, D.-J. Kim, O.-P. Kwon
Department of Molecular Science and Technology
Ajou University
Suwon 16499, Korea
E-mail: opilkwon@ajou.ac.kr

I. C. Yu, F. Rotermund
Department of Physics
Korea Advanced Institute of Science and Technology (KAIST)
Daejeon 34141, Korea
E-mail: rotermund@kaist.ac.kr

The ORCID identification number(s) for the author(s) of this article can be found under https://doi.org/10.1002/adfm.202209915.

DOI: 10.1002/adfm.202209915

M. Jazbinsek
Institute of Computational Physics
Zurich University of Applied Sciences (ZHAW)
8401 Winterthur, Switzerland

W. Yoon, H. Yun
Department of Chemistry & Department of Energy Systems Research
Ajou University
Suwon 16499, Korea

D. Kim
Department of Chemistry
Kyonggi University
San 94–6, Iui-dong, Yeongtong-gu, Suwonsi, Gyeonggi 443–760, Korea

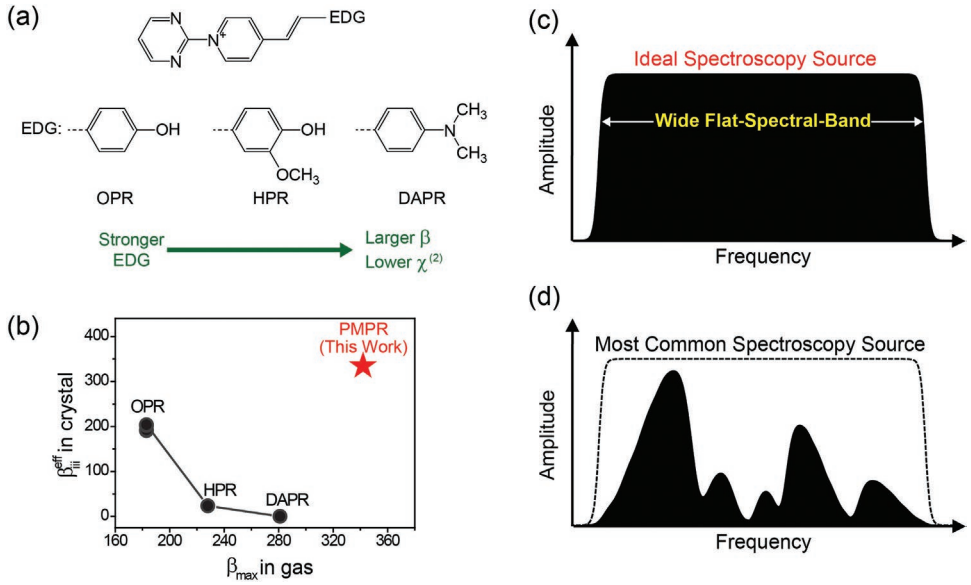


**Scheme 1.** a) Previously reported *N*-pyrimidinyl stilbazolium chromophores (OPR, HPR, and DAPR) with various electron donating groups (EDGs) and b) their molecular optical nonlinearity (maximum first hyperpolarizability $\beta_{max}$ in gas phase) and macroscopic optical nonlinearity (effective first hyperpolarizability $\beta_{iii}^{eff}$ in crystals).[15–17] For comparison, newly designed PMPR chromophore in this work is also presented. Schematic of c) ideal spectroscopy source with wide flat-spectral-band and d) most common source with absorption dimples for broadband THz spectroscopy.

to zero macroscopic second-order optical nonlinearity. The first hyperpolarizability of push–pull chromophores generally increases with increasing electron donating strength of electron donating groups (EDGs).[2,13,14] For instance, for *N*-pyrimidinyl stilbazolium chromophores, the maximum first hyperpolarizability $\beta_{max}$ in gas phase increases with increasing the strength of EDGs in the order of 4-hydroxyphenyl, 4-hydroxy-3-methoxyphenyl, and 4-dimethylaminophenyl groups for OPR ((4-hydroxystyryl)-1-(pyrimidin-2-yl)pyridinium), HPR (4-(4-hydroxy-3-methoxystyryl)-1-(pyrimidin-2-yl)pyridinium), and DAPR (4-(4-(dimethylamino)styryl)-1-(pyrimidin-2-yl)pyridinium) chromophores, respectively (see **Scheme 1**a,b). However, the macroscopic optical nonlinearity (which scales with the effective first hyperpolarizability $\beta_{iii}^{eff}$) in crystals decreases with increasing molecular optical nonlinearity $\beta_{max}$.[15–17] Eventually, although the DAPR chromophore introducing the strongest electron donating dialkylamino EDG exhibits the largest molecular optical nonlinearity $\beta_{max}$, DAPR crystals exhibit centrosymmetric crystal structure with zero effective first hyperpolarizability $\beta_{iii}^{eff}$.[15]

It is well known since two decades that the DAPR chromophore, consisting of *N*-pyrimidinyl stilbazolium and dialkylamino EDG, exhibits extremely large molecular optical nonlinearity that is up to several times higher than that of the benchmark 4-(4-(dimethylamino)styryl)-1-methylpyridinium 4-methylbenzenesulfonate (DAST) crystals.[15,18–20] However, DAPR and analogous crystals possessing large macroscopic optical nonlinearity have never been reported yet. Herein, to the best of our knowledge, we report the first DAPR analogous crystals that exhibit extremely large macroscopic optical nonlinearity.

In this work, we newly designed the cationic chromophore PMPR (4-(4-(4-(hydroxymethyl)piperidin-1-yl)styryl)-1-(pyrimidin-2-yl)pyridin-1-ium, **Figure 1**a) possessing extremely large, top-level molecular optical nonlinearity (Scheme 1b). In crystals, incorporating a head-to-tail cation-anion O—H···O hydrogen-bonding synthon and selecting an optimal molecular anion result in extremely large effective first hyperpolarizability $\beta_{iii}^{eff}$ of $335 \times 10^{-30}$ esu. This is about double the value achieved in benchmark DAST crystals with $\beta_{iii}^{eff} = 161 \times 10^{-30}$ esu.[20,21] Based on the large macroscopic optical nonlinearity, as-grown PMPR-based crystal with an ultrathin thickness of ≈10 µm shows excellent THz generation performance; both broadband generation with a wide flat-spectral-band and high-generation efficiency. It satisfies the requirements of an ideal THz source for broadband THz spectroscopy. Therefore, PMPR crystals are very promising materials for THz photonic and other nonlinear optical applications.

## 2. Results and Discussion

### 2.1. Design for Overcoming the Bottleneck in Nonlinear Optics

Figure 1a shows the chemical structure of the newly designed PMPR cation and two molecular counter anions, MO (4-((4-(dimethylamino)phenyl)diazenyl)benzenesulfonate) and CBS (4-chlorobenzenesulfonate). For designing the new PMPR cationic chromophore, we considered i) boosting molecular optical nonlinearity and simultaneously ii) introducing a hydrogen-bond donor group to promote a head-to-tail cation-anion O—H···O hydrogen-bonding synthon that may induce non-centrosymmetric ordering of chromophores in the crystalline state. To obtain large molecular optical nonlinearity, a strong EDG, the piperidino group on piperidin-4-ylmethanol (PM) group and a strong electron withdrawing group (EWG), the *N*-pyrimidinyl pyridinium (PR) groups are introduced at the ends of the PMPR chromophore. Since PMPR and DAPR chromophores have an analogous EDG, piperidino and

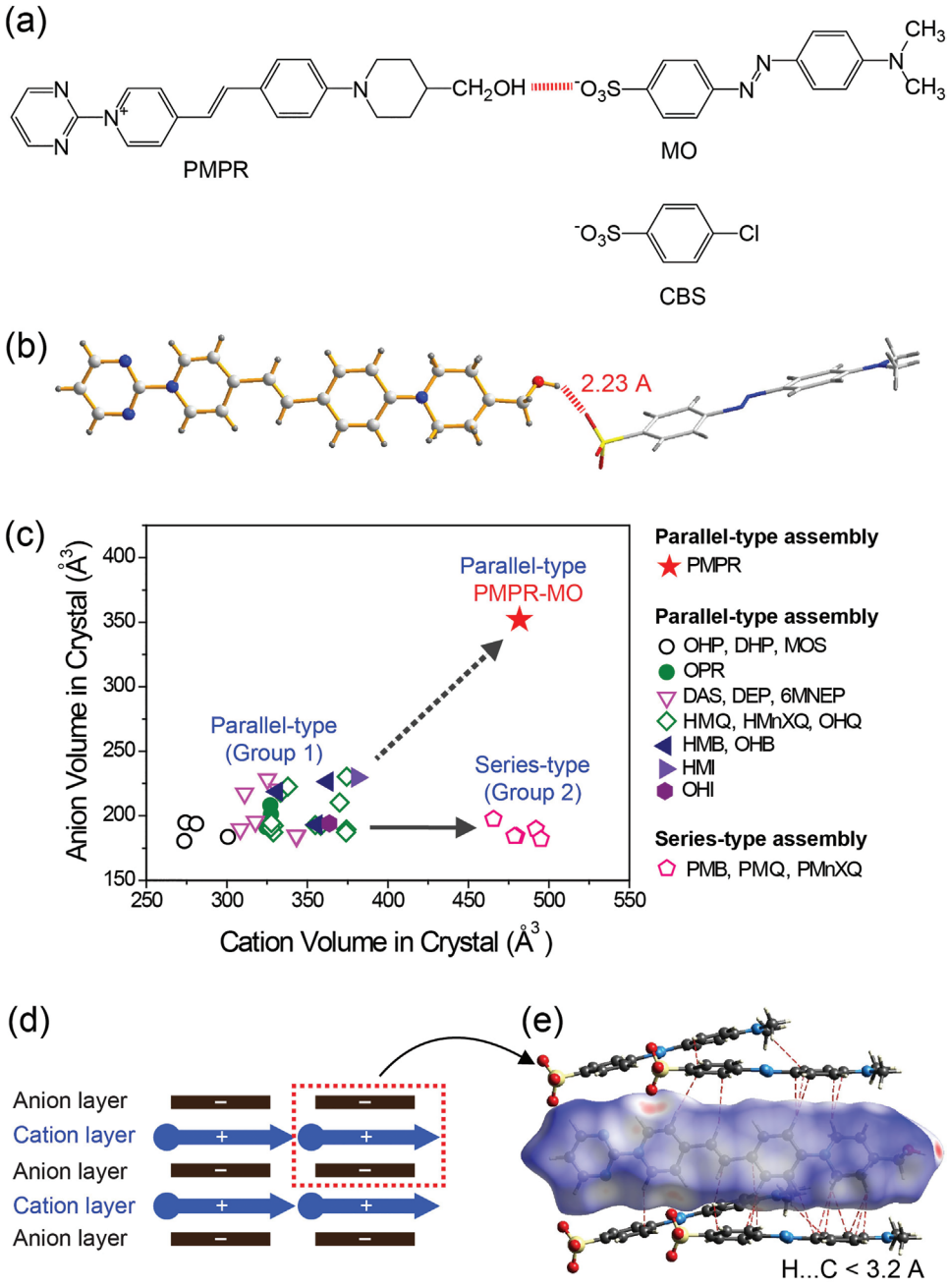


**Figure 1.** a) Newly designed PMPR-MO and PMPR-CBS. b) Head-to-tail cation-anion assembly based on strong hydrogen bond between —OH···—$O_3$S— groups in PMPR-MO(I) crystals. c) Crystallographic volume of molecular cations and anions in benchmark organic nonlinear optical crystals, determined from Hirshfeld surface analysis. d) Schematic of parallel-type assembly in benchmark organic salt crystals. e) Hirshfeld surface of PMPR cation, presenting X···Y close contacts of H···C (≤3.2 Å, red dotted lines), in PMPR-MO(I) crystals.

dialkylamino group, respectively, the PMPR chromophore is expected to possess a large molecular optical nonlinearity like the DAPR chromophore.

For achieving non-centrosymmetric ordering of PMPR chromophores in the crystalline state by incorporating a head-to-tail cation-anion O—H···O hydrogen-bonding synthon, hydrogen-bond donor and acceptor groups are introduced into cation and anion, respectively. The aliphatic hydroxyl —OH ($\delta$+) group on PM EDG at an end of PMPR cations and the negative O atoms on aromatic sulfonate group at an end of MO (and CBS) anions can act as hydrogen-bond donor and acceptor, respectively, as shown in Figure 1a.[22–25] We explore here two molecular counter anions with a different size; the bigger MO anion and the smaller CBS anion.

New PMPR-MO and PMPR-CBS were synthesized by the metathesis reaction of PMPR chloride (PMPR-Cl) and the corresponding sodium aromatic sulfonate (or silver aromatic sulfonate). The details of the synthesis, crystallization processes,

and crystal structure and symmetry analysis are described in the Supporting Information. PMPR-MO exhibits polymorphism at our experimental conditions; two polymorphs, PMPR-MO(I) and PMPR-MO(II) were observed as shown in Figure S1 (Supporting Information). In contrast, we did not observe polymorphism for PMPR-CBS.

Although PMPR-MO and PMPR-CBS consist of an identical PMPR chromophore and an identical head-to-tail cation-anion O—H···O hydrogen-bonding synthon, their crystal symmetry can be different. It is because the molecular MO and CBS anions possess a substantially different size that may additionally contribute to interionic interactions. In qualitative powder second harmonic generation (SHG) measurements[26,27] at the fundamental wavelength of 1300 nm, PMPR-CBS powder shows no measurable SHG signal expected at 650 nm, but a clear third harmonic generation (THG) signal at 433 nm as shown in Figure S3 (Supporting Information). Two polymorphs of PMPR-MO exhibit different results; PMPR-MO(I) powder shows a strong SHG signal, while PMPR-MO(II) powder shows no SHG signal. These results indicate that PMPR-CBS and PMPR-MO(II) possess a centrosymmetric, while PMPR-MO(I) a non-centrosymmetric crystal structure with a second-order nonlinear optical functionality.

To investigate the details of the molecular ordering in PMPR-MO crystals, we grow single crystals of PMPR-MO(I) and PMPR-MO(II) phases. PMPR-MO(I) crystals exhibit non-centrosymmetric monoclinic *Pc* space group symmetry and PMPR-MO(II) crystals exhibit centrosymmetric triclinic $P\bar{1}$ space group symmetry. The corresponding molecular ordering of PMPR-MO(I) and PMPR-MO(II) crystals is presented in **Figure 2** and Figure S2 (Supporting Information), respectively. Importantly, PMPR-MO(I) crystals have an optimal molecular ordering of PMPR chromophores for second-order nonlinear optics; a (close-to) perfect parallel alignment of PMPR chromophores (Figure 2). PMPR-MO(I) crystals exhibit head-to-tail self-assembly between PMPR cations and MO anions (Figure 1b). A pair of PMPR cationic chromophore and MO anion forms a strong hydrogen bond between the $-OH\cdots{}^{-}O_3S-$ groups with a very short distance of 2.23 Å. As a consequence, among three crystalline phases of PMPR-based crystals, PMPR-MO(I) crystals are highly attractive for macroscopic second-order nonlinear optical applications.

The reason of obtaining different crystal symmetry in non-centrosymmetric PMPR-MO(I) and centrosymmetric PMPR-CBS crystals may be attributed to the size of molecular anions. To explore this hypothesis, we analyze the crystallographic

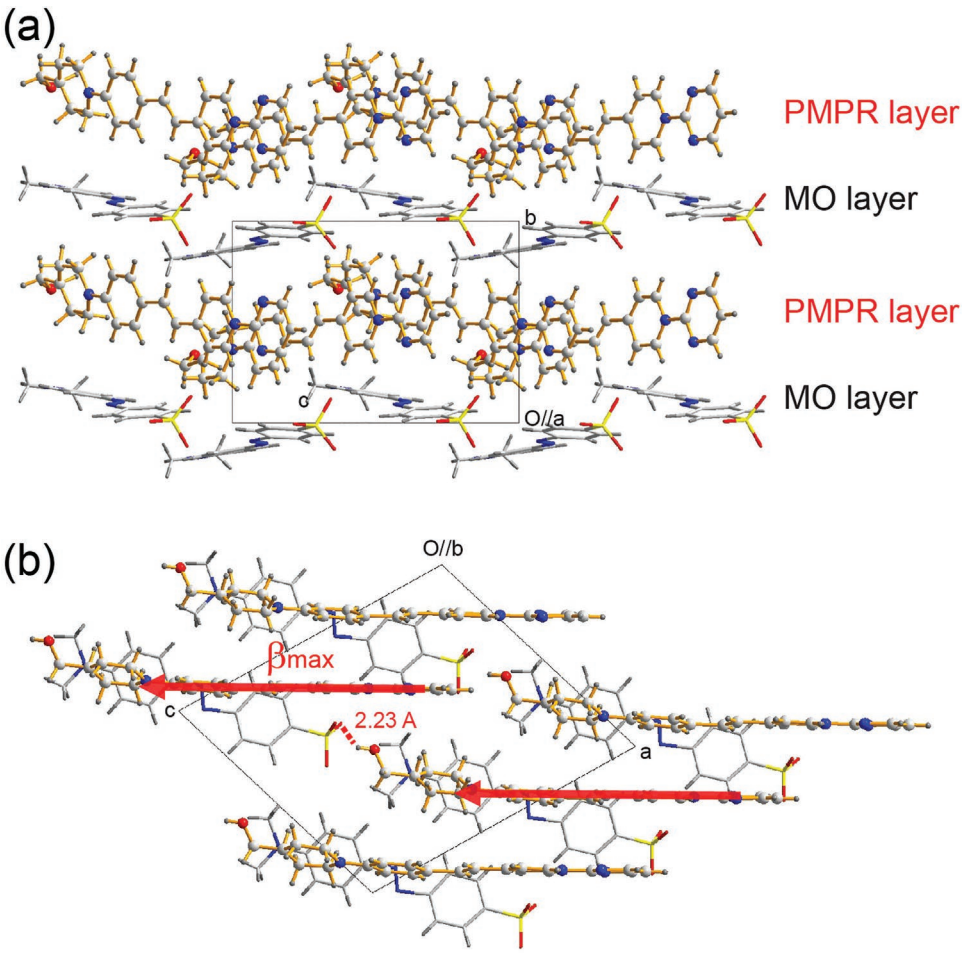


**Figure 2.** Molecular ordering of PMPR-MO (I) crystals with monoclinic *Pc* space group. The solid arrows present the direction of the first hyperpolarizability $\beta_{max}$ of PMPR cations.

volume of cationic chromophores and anions in benchmark organic nonlinear optical salt crystals with high-order parameter,[16,20,22–24,28–51] by using the Hirshfeld surface analysis.[52–54] The results are plotted in Figure 1c. Note that the previously reported benchmark organic nonlinear optical salt crystals having a high-order parameter close to the maximum value (≈1.0) can be classified into two groups; parallel- and series-type assemblies.[9] In this work, Group 1 and 2 crystals correspond to parallel- and series-type assemblies, respectively (see Figure 1c).

In parallel-type assembly in benchmark crystals, cationic chromophore layers are surrounded by anionic layers as shown in Figure 1d. Group 1 crystals are based on many cationic chromophores; DAS (4-(4-(dimethylamino)styryl)-1-methylpyridinium), OHP (4-(4-hydroxystyryl)-1-methylpyridinium), DHP (4-(3,4-dihydroxystyryl)-1-methylpyridinium), MOS (4-(4-methoxystyryl)-1-methylpyridinium), OPR, DEP (4-((4-(dimethylamino)phenyl)ethynyl)-1-methylpyridin-1-ium), 6MNEP (4-(2-(6-methoxynaphthalen-2-yl)vinyl)-1-methylpyridinium), HMQ (2-(4-hydroxy-3-methoxystyryl)-1-methylquinolinium), HMnXQ (halogenated 2-(4-hydroxy-3-methoxystyryl)-1-methylquinolinium), OHQ (2-(4-hydroxystyryl)-1-methylquinolinium), HMB (2-(4-hydroxy-3-methoxystyryl)-3-methylbenzothiazol-3-ium), OHB (2-(4-hydroxy-3-methoxystyryl)-3-methylbenzothiazol-3-ium), HMI (2-(4-hydroxy-3-methoxystyryl)-1,3-dimethyl-1H-benzoimidazol-3-ium), and OHI (2-(4-hydroxystyryl)-1,3,3-trimethyl-3H-indolium).[17,20,28–50] Interestingly, for Group 1 crystals, the crystallographic volume of both cationic chromophores and counter anions is within a very narrow range; ≈270–380 and ≈180—230 Å$^3$, respectively.

For cationic chromophores of a larger size (e.g., PMB (2-(4-(4-(hydroxymethyl)piperidin-1-yl)styryl)-3-methylbenzothiazol-3-ium), PMQ (2-(4-(4-(hydroxymethyl)piperidin-1-yl) styryl)-1-methyl-quinolinium), and PMnXQ (halogenated 2-(4-(4-(hydroxymethyl)piperidin-1-yl)styryl)-1-methyl-quinolinium)), the assembling changed; from parallel-type assembly to series-type assembly (i.e., Group 2 in Figure 1c).[22–24,51] This shows that a proper balance between the volume of cation and anion may be needed for obtaining a high-order parameter (i.e., large macroscopic optical nonlinearity).

In PMPR-MO(I) crystals, PMPR cation layers are surrounded by MO anionic layers (Figure 1e). This is a typical feature of parallel-type assembly. In PMPR-MO(I) crystals, PMPR cationic chromophore possesses a much bigger crystallographic volume (482 Å$^3$) compared to the cationic chromophores in Group 1 (≈270—380 Å$^3$). For surrounding PMPR cations by anions, longer MO anions compared to CBS anions may be advantageous for formation of parallel-type assembly. If PMPR cations were surrounded by small CBS counter anions in the formation of parallel-type assembly, CBS anion layers could not fully surround PMPR cationic layers, which would result in many empty spaces in crystals, i.e., an unfavorable molecular ordering in the crystalline state. Therefore, PMPR-MO(I) crystals having parallel-type assembly present a new class of organic crystals having top-level macroscopic optical nonlinearity; different to previously reported benchmark crystals (Group 1 and 2 in Figure 1c).

### 2.2. Extremely Large Macroscopic Hyperpolarizability

As mentioned above, the PMPR chromophore is an analog to the DAPR chromophore. The DAPR cationic chromophore exhibits a very large molecular optical nonlinearity; e.g., the first hyperpolarizability $\beta_{HRS}$ of $1015 \times 10^{-30}$ esu obtained from hyper-Rayleigh scattering (HRS) in acetonitrile solution at 1300 nm fundamental wavelength[18] and the maximum (nonresonant) first hyperpolarizability $\beta_{max}$ of $281 \times 10^{-30}$ esu as evaluated in this work (Scheme 1). Therefore, the PMPR cationic chromophore is also expected to possess a large molecular optical nonlinearity. In addition, since PMPR-MO(I) crystals exhibit a (close-to) perfectly parallel ordering of PMPR chromophores, they must possess a large macroscopic optical nonlinearity. In this work, to evaluate the macroscopic optical nonlinearity of PMPR-MO(I) crystals, we calculated the maximum first hyperpolarizability $\beta_{max}$ of PMPR chromophore having an optimized conformation (OPT) using density functional theory calculations and then consider the orientation of PMPR chromophores in the crystalline state.[21,37] The details are described in the Supporting Information. In previous reports, this method has shown a good agreement with experimental macroscopic nonlinear optical response.[30,55]

**Figure 3**a shows the frontier molecular orbitals (FMOs) for PMPR chromophore optimized at the B3LYP/6-311+G(d,p) level. For PMPR chromophore, the highest occupied molecular orbital (HOMO) and the lowest unoccupied molecular orbital (LUMO) are effectively delocalized and look quite similar in particular for the central styryl group. This indicates that they arise from significant electronic couplings between the fragment molecular orbitals of the central styryl group and neighboring substituents. We also note, however, that the HOMO and LUMO have more significant weights in the electron-donating piperidino and strong electron-withdrawing *N*-pyrimidinyl pyridinium groups, respectively, and thus are effectively separated. Such an orbital separation in PMPR chromophore is discerned clearer when the HOMO-1 and LUMO+1 states are compared. All these add up to a conclusion that the PMPR chromophore is a push-pull type $\pi$-conjugated chromophore and exhibits an efficient delocalization of $\pi$-electrons, which may result in large molecular optical nonlinearity.

PMPR cationic chromophore exhibits an extremely large maximum first hyperpolarizability $\beta_{max}$ (OPT); $342 \times 10^{-30}$ esu. The measured wavelength of maximum absorption $\lambda_{max}$ for PMPR chromophore is also very high, 553 nm in methanol (Figure 3b), which confirms the high-molecular nonlinearity according to the general nonlinearity-transparency trade-off.[13] These values ($\beta_{max}$ (OPT) and $\lambda_{max}$) are remarkably higher than the corresponding values for the chromophore DAS used in benchmark 4-(4-(dimethylamino)styryl)-1-methylpyridinium 4-methylbenzenesulfonate (DAST) crystals ($\beta_{max}$ (OPT) = $159 \times 10^{-30}$ esu and $\lambda_{max}$ = 475 nm).[21] Moreover, they are also significantly higher than those of previously reported *N*-pyrimidinyl stilbazolium OPR chromophore having relatively weak electron-donating phenolic group ($\beta_{max}$ (OPT) = $183 \times 10^{-30}$ esu and $\lambda_{max}$ = 443 nm).[17]

The molecular ordering angle $\theta_p$, i.e., the angle between the direction of $\beta_{max}$ and the symmetry *ac* crystallographic plane for

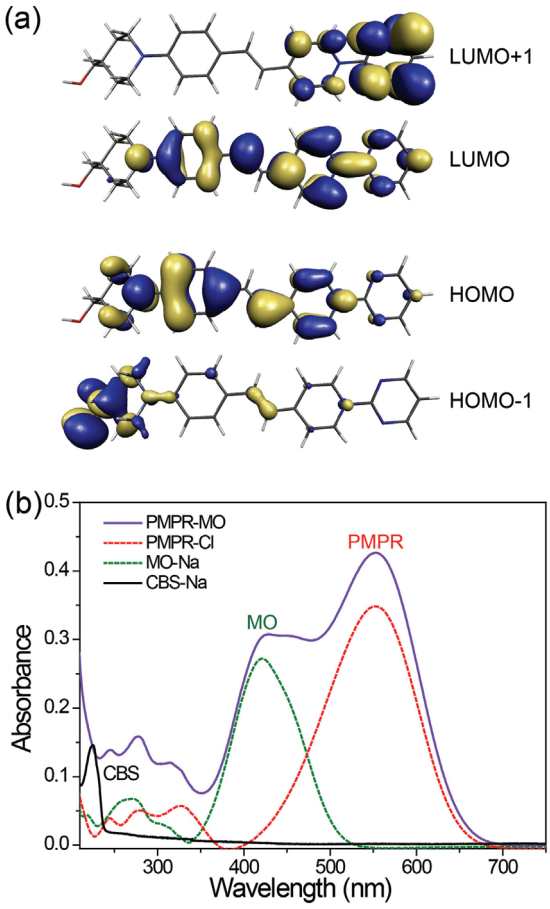


**Figure 3.** a) Frontier molecular orbital pairs at B3LYP/6-311+g(d,p) for PMPR chromophore. b) Absorption spectra of PMPR-MO, PMPR-Cl, MO-Na, and CBS-Na in methanol ($10^{-5}$ M).

PMPR-MO(I) crystals is very small; ≈7°. This means that the molecular ordering of PMPR chromophores is close-to optimal for maximizing the macroscopic optical nonlinearity of PMPR-MO(I) crystals. The corresponding macroscopic optical nonlinearity is therefore extremely large for PMPR-MO(I) crystals. The diagonal component of the effective first hyperpolarizability $\beta_{iii}^{eff} = \beta_{max}(OPT) \cdot \cos^3\theta_p$ is $335 \times 10^{-30}$ esu. This is about twice as large as in benchmark DAST crystals ($161 \times 10^{-30}$ esu).[21] Therefore, PMPR-MO(I) crystals with extremely large diagonal effective first hyperpolarizability $\beta_{iii}^{eff}$ are very interesting materials for various nonlinear optical applications. In addition, PMPR-MO(I) crystals exhibit a high thermal stability up to ≈260 °C as shown in Figure S4 (Supporting Information).

### 2.3. Efficient THz Wave Generation with Wide Flat-Spectral-Band

Large macroscopic second-order optical nonlinearity of organic crystals is highly beneficial to enhance the performance of diverse nonlinear optical devices. In THz wave generation, the optical-to-THz frequency conversion efficiency is proportional to the square of the macroscopic nonlinear optical coefficient of source materials.[9,10] Since PMPR-MO(I) crystals possess a very large nonlinear optical coefficient ($\beta_{iii}^{eff} = 335 \times 10^{-30}$ esu),

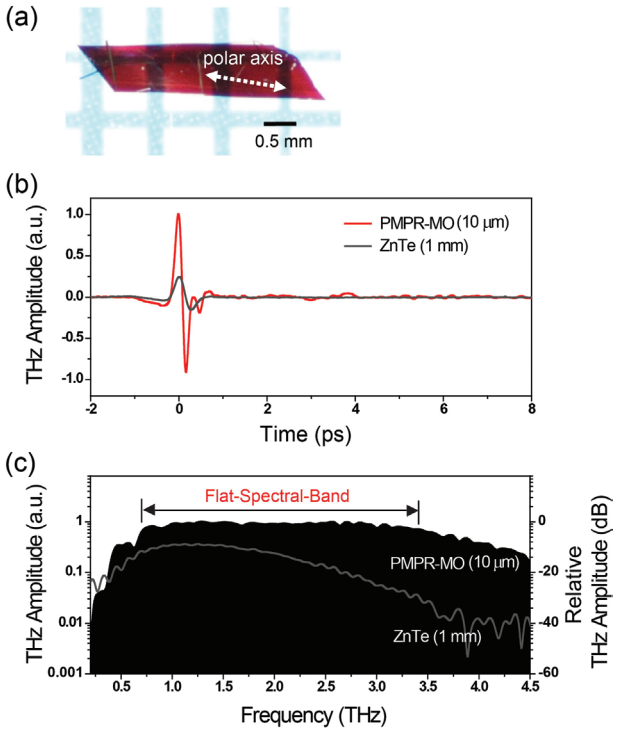


**Figure 4.** a) Ultrathin PMPR-MO(I) crystal with a thickness of ≈10 μm (see Figure S5, Supporting Information, for the side view). THz generation in 10 μm thick PMPR-MO(I) and 1.0 mm thick ZnTe crystals, pumped at 1300 nm: b) time traces and c) the corresponding generated spectra, for which full spectra up to 8 THz are shown in Figure S6 (Supporting Information). The THz amplitude is normalized to 1.0 for the highest THz amplitude of PMPR-MO(I). The flat-spectral-band is here defined between the highest and lowest THz frequencies at −3 dB of the highest THz amplitude.

PMPR-MO(I) may act as an efficient THz wave generator with high-conversion efficiency.

**Figure 4**a shows a photograph of an as-grown PMPR-MO(I) single crystal with an area of a few $mm^2$. This shows that PMPR-MO(I) has bulk crystal growth ability. Among organic crystals having large nonlinear optical coefficient, many crystals unfortunately exhibit poor growing ability for bulk crystals with a lateral size over mm-scale. Possessing bulk crystal growth ability for PMPR-MO(I) crystals is highly beneficial for real-world optical applications. The thickness of the as-grown PMPR-MO(I) single crystal is ultrathin; ≈10 μm and exhibit a strong optical anisotropy (Figure S5, Supporting Information). The high anisotropy of PMPR-MO(I) single crystal originates from the parallel alignment of PMPR cations and MO anions (Figure 2a). Organic crystals both possessing an ultrathin thickness and a large nonlinear optical coefficient show advantages for THz wave generation (i.e., dimple-free broad spectral bandwidth with high generation efficiency) as discussed below.

Using very thin THz source materials in the range from few μm to few tens of μm is a very attractive approach for achieving broadband THz wave generation. This is because an ultrathin thickness can overcome the bandwidth limitations due to self-absorption and phase-mismatch between the used optical pump and the generated THz waves.[9,56] However, although very thin THz source materials can generate spectra with an

ultra-broad bandwidth of THz waves, the resulting THz generation efficiency is in most cases very low compared to thicker crystals. This is because the generated THz amplitude is proportional to the thickness of THz source materials within the coherence length.[9] For example, widely used inorganic semiconducting THz source materials including GaAs, ZnTe, and GaP crystals were shown to generate broadband THz waves by using a very thin thickness, but with a very low THz conversion efficiency.[9] The conversion efficiency in this case is also limited by the macroscopic optical nonlinearity of inorganic semiconductors (e.g., ≈4 pm/V for ZnTe), which is one order of magnitude smaller than that of benchmark organic crystals. For thicker ZnTe crystals in the mm-scale (e.g., 1.0 mm), the bandwidth of the generated THz waves is limited with an upper cut-off generation frequency of <3 THz.[8] Consequently, as-grown PMPR-MO(I) single crystals having both an ultrathin thickness and a large nonlinear optical coefficient are promising materials to generate THz waves with a broad, dimple-free spectrum, and a high-conversion efficiency.

To show the potential of PMPR-MO(I) crystals, THz wave generation experiments were performed with an ultrathin PMPR-MO(I) single crystal having a thickness of 10 μm and the result was compared with that achieved in a 1.0 mm thick ZnTe crystal. Near-infrared optical pulses at 1300 nm with a pulse duration of 140 fs at 1-kHz repetition rate were used as pump to generate THz waves in crystals by optical rectification. The pump beam diameter was ≈0.5 mm at the average pump power of 10 mW. The generated THz waves were detected via EOS in a 0.3 mm thick GaP, where 800 nm pulses with 100 fs pulse duration were used to measure the THz electric field.

Figure 4b,c shows the time traces and the corresponding spectra of the generated THz waves in PMPR-MO(I) and in reference ZnTe crystal. Although PMPR-MO(I) crystal has an ultrathin thickness of ≈10 μm, the generated THz amplitude is very high. Compared to the much thicker ZnTe crystal (1.0 mm), the peak-to-peak THz field generated in the 10 μm thick PMPR-MO(I) crystal is 4.6 times higher. The results confirm that a very high optical-to-THz conversion efficiency could be achieved with PMPR-MO(I) crystal, which originates from its exceptionally large macroscopic optical nonlinearity. This high optical-to-THz conversion efficiency of only a 10 μm thick PMPR-MO(I) crystal is outstanding; many organic benchmark THz-generation crystals with the thickness of few hundred micrometers generate about one order of magnitude higher THz electric-field than ZnTe (1.0 mm) at very similar experimental conditions with this work.[9]

Furthermore, the THz waves generated in PMPR-MO(I) crystal show a very flat, dimple-free broadband spectrum. As shown in Figure 4c, the generated THz waves exhibit an extremely broad flat spectral band in the frequency range of 0.7–3.4 THz. The flat-spectral-band in the present work is defined as the frequency range, for which the difference between the highest and the lowest THz amplitude is below 3 dB. Note that this is comparable or even better than the preferred spectral bandwidth, shape, and extinction ratio of conventional band-pass filters. As illustrated in Scheme 1c, an ideal spectroscopic source should provide as broad and as flat spectral band as possible for application in broadband (THz) spectroscopy.

In addition, the entire THz spectrum from PMPR-MO(I) crystal does not show strong dimples. In most organic THz generators, many dimples usually appeared as illustrated in Scheme 1d. Moreover, the total useful bandwidth of the generated THz spectrum from PMPR-MO(I) crystal is extremely broad at the pump pulse duration of 140 fs. The upper cut-off generation frequency is ≈7 THz as shown in Figure S6 (Supporting Information). Figure S7 (Supporting Information) shows the measured absorbance of a PMPR-MO(I) single crystal along the polar axis in THz frequency range. The absorbance of as-grown ultrathin 10 μm thick PMPR-MO(I) crystal is very small; only very broad and small peaks at 2.0 and 4.5 THz were observed. In many benchmark organic THz generators with the thickness over hundred micrometers, the self-absorption in the THz frequency range due to phonon/vibrational modes was shown to limit the generated THz spectral bandwidth and cause undesired spectral dimples.[9,56] However, with ultrathin organic crystals (10 μm as in this work), the influence of self-absorption on THz-wave generation characteristics may be negligible because of a relatively very small absorption (Figure S7, Supporting Information). Note that even in much thicker benchmark organic THz-generation crystals with a thickness of 100 μm, the reduction of the generated THz spectrum by self-absorption was already reported to be very small.[56] Ultrathin thickness of PMPR-MO(I) single crystals is therefore highly beneficial to obtain a very flat and broadband THz generation spectrum without strong dimples. Consequently, PMPR-MO(I) single crystal with an ultrathin thickness of 10 μm and the extremely large diagonal component of the effective first hyperpolarizability $\beta_{iii}^{eff}$ enabled us to simultaneously achieve i) a well-defined dimple-free flat THz spectrum and ii) a high optical-to-THz frequency conversion efficiency.

### 2.4. Crystal Characteristics

For practical applications including THz-wave generation, other crystal characteristics beyond the large macroscopic optical nonlinearity are important. Figure S8 (Supporting Information) shows the result of a hygroscopy test of PMPR-MO(I) crystal on a water droplet. PMPR-MO(I) crystals show high-water resistance; i.e., a high environmental stability against humidity. Note that many organic nonlinear optical salt crystals are highly soluble in water and may even exhibit a phase transition to a hydrated phase (DAST for example).

In addition, obtaining ultrathin thickness (e.g., 10 μm as shown in Figure S5, Supporting Information) of as-grown PMPR-MO(I) single crystals is highly beneficial. Note that the growth of ultrathin organic nonlinear optical single crystals with few micrometers to few tens of micrometers is very difficult and usually required special crystal growth techniques.[32,57,58] Moreover, simultaneous achievement of a relative large area over few $mm^2$ scale is also very interesting for various (nonlinear optical) photonic applications.[1,3,9,32,59,60] The thin plate morphology of as-grown PMPR-MO(I) single crystals is suitable for diverse optical experiments without additional polishing and cutting processes, as used in our THz generation experiments. Consequently, PMPR-MO(I) single crystals having extremely large diagonal optical nonlinearity exhibit

high-environmental stability and good crystal growing ability resulting in ultrathin single crystals with the area of over few $mm^2$.

## 3. Conclusion

In summary, we have newly developed highly efficient second-order nonlinear optical organic crystals based on *N*-pyrimidinyl stilbazolium PMPR chromophores possessing extremely large maximum first hyperpolarizability $\beta_{max}$ of $342 \times 10^{-30}$ esu. Incorporating a highly nonlinear PMPR cationic chromophore, a head-to-tail cation-anion O—H···O hydrogen-bonding synthon, and an optimal selection of the counter anion with an appropriate size result in extremely large macroscopic optical nonlinearity with the effective first hyperpolarizability $\beta_{iii}^{eff}$ of $335 \times 10^{-30}$ esu. To the best of our knowledge, this is the first report of organic crystals having such an extremely large effective first hyperpolarizability $\beta_{iii}^{eff} > 300 \times 10^{-30}$ esu and a bulk crystal growth ability. Based on this extremely large macroscopic optical nonlinearity and an ultrathin thickness, PMPR-MO single crystal allows us to generate dimple-free broadband THz waves with a wide flat-spectral-band in the range of 0.7–3.4 THz at −3 dB, a large upper cut-off frequency of > 7 THz and a high-generation efficiency. Therefore, new class of organic nonlinear optical PMPR-MO crystals are very interesting materials for practical nonlinear optical applications. In addition, the design approach we applied for PMPR-MO crystals (incorporating cation-anion O—H···O hydrogen-bonding synthon and anion selection with an optimal size) may be very beneficial for designing further highly efficient organic crystals based on chromophores possessing extremely large molecular optical nonlinearity.

## 4. Experimental Section

The details of synthesis, crystallization process, X-ray crystal structure analysis, powder SHG measurements, optical nonlinearity, thermal stability, crystal morphology, and THz wave generation are described in the Supporting Information.

## Supporting Information

Supporting Information is available from the Wiley Online Library or from the author.

## Acknowledgements

S.J.K. and I.C.Y. contributed equally to this work. This work was supported by the National Research Foundation of Korea (NRF) funded by the Ministry of Science, ICT & Future Planning, Korea (No. 2021R1A2C1005012, 2021R1A5A6002853, 2019K1A3A1A14057973, and 2019R1A2C3003504), Institute of Information & communications Technology Planning & Evaluation (IITP) grant funded by the Korea government (MSIT) (No. 2022-0-00624) and Swiss National Science Foundation (SNSF), Switzerland (No. IZKSZ2_188194). X-ray structural analysis was supported by Basic Science Research Program through the National Research Foundation of Korea(NRF) funded by the Ministry of Education (2019R1I1A2A01058066).

## Conflict of Interest

The authors declare no conflict of interest.

## Data Availability Statement

Research data are not shared.

## Keywords

electro-optics, nonlinear optics, THz photonics

Received: August 27, 2022
Revised: October 3, 2022
Published online: October 31, 2022

[1] Q. Ma, A. G. Grushin, K. S. Burch, *Nat. Mater.* **2021**, *20*, 1601.
[2] H. Xu, D. L. Elder, L. E. Johnson, Y. De Coene, S. R. Hammond, W. V. Ghinst, K. Clays, L. R. Dalton, B. H. Robinson, *Adv. Mater.* **2021**, *33*, 2104174.
[3] G. Lu, J. Hong, F. Qiu, A. M. Spring, T. Kashino, J. Oshima, M. Ozawa, H. Nawata, S. Yokoyama, *Nat. Commun.* **2020**, *11*, 4224.
[4] Y. Enami, C. T. D. , D. Mathine, C. Loychik, C. Greenlee, R. A. Norwood, T. D. Kim, J. Luo, Y. Tian, A. K.-Y. Jen, N. Peyghambarian, *Nat. Photonics* **2007**, *1*, 180.
[5] L. Chang, S. Liu, J. E. Bowers, *Nat. Photonics* **2022**, *16*, 95.
[6] B. Zhang, L. Wang, F. Chen, *Laser Photonics Rev.* **2020**, *14*, 1900407.
[7] M. Annadhasan, S. Basak, N. Chandrasekhar, R. Chandrasekar, *Adv. Opt. Mater.* **2020**, *8*, 2000959.
[8] J. A. Fülöp, S. Tzortzakis, T. Kampfrath, *Adv. Opt. Mater.* **2020**, *8*, 1900681.
[9] S. J. Kim, B. J. Kang, U. Puc, W. T. Kim, M. Jazbinsek, F. Rotermund, O. P. Kwon, *Adv. Opt. Mater.* **2021**, *9*, 2101019.
[10] J. Hebling, K. L. Yeh, M. C. Hoffmann, B. Bartal, K. A. Nelson, *J. Opt. Soc. Am. B.* **2008**, *25*, B6.
[11] M. Martin, J. Mangeney, P. Crozat, P. Mounaix, *Appl. Phys. Lett.* **2010**, *97*, 111112.
[12] A. Schneider, I. Biaggio, P. Günter, *Appl. Phys. Lett.* **2004**, *84*, 2229.
[13] O.-P. Kwon, S.-J. Kwon, M. Jazbinsek, F. D. J. Brunner, J.-I. Seo, C. Hunziker, A. Schneider, H. Yun, Y.-S. Lee, P. Günter, *Adv. Funct. Mater.* **2008**, *18*, 3242.
[14] Ch. Bosshard, M. Bösch, I. Liakatas, M. Jäger, in *Nonlinear Optical Effects and Materials*, Ch.3 (Ed: P. Günter), Springer-Verlag, Berlin **2000**.
[15] L. R. Dalton, P. A. Sullivan, D. H. Bale, *Chem. Rev.* **2010**, *110*, 25.
[16] B. J. Coe, J. A. Harris, I. Asselberghs, K. Clays, G. Olbrechts, A. Persoons, J. T. Hupp, R. C. Johnson, S. J. Coles, M. B. Hursthouse, K. Nakatani, *Adv. Funct. Mater.* **2002**, *12*, 110.
[17] B. R. Shin, S. I. Kim, D. W. Kim, M. Jazbinsek, W. J. Yoon, H. S. Yun, I. C. Yu, F. Rotermund, O. P. Kwon, *Opt. Laser Technol.* **2022**, *156*, 108454.
[18] S. J. Kim, S. I. Kim, M. Jazbinsek, W. J. Yoon, H. S. Yun, D. W. Kim, I. C. Yu, F. Rotermund, O. P. Kwon, *Adv. Photonics Res.* **2022**, *3*, 2100350.
[19] B. J. Coe, J. A. Harris, I. Asselberghs, K. Clays, G. Olbrechts, A. Persoons, J. T. Hupp, R. C. Johnson, S. J. Coles, M. B. Hursthouse, K. Nakatani, *Adv. Funct. Mater.* **2002**, *12*, 110.
[20] B. J. Coe, D. Beljonne, H. Vogel, J. Garin, J. Orduna, *J. Phys. Chem. A* **2005**, *109*, 10052.
[21] S. R. Marder, J. W. Perry, W. P. Schaefer, *Science* **1989**, *245*, 626.

[22] P. J. Kim, J. H. Jeong, M. Jazbinsek, S. J. Kwon, H. Yun, J. Kim, Y. S. Lee, I. H. Baek, F. Rotermund, P. Günter, O. P. Kwon, *CrystEngComm* **2011**, *13*, 444.
[23] J. H. Seok, D. J. Kim, W. T. Kim, S. J. Kim, W. J. Yoon, G. E. Yoon, I. C. Yu, M. Jazbinsek, S. W. Kim, H. S. Yun, D. W. Kim, F. Rotermund, O. P. Kwon, *Adv. Opt. Mater.* **2021**, *9*, 2100324.
[24] S. C. Lee, B. J. Kang, J. A. Lee, S. H. Lee, M. Jazbinšek, W. Yoon, H. Yun, F. Rotermund, O. P. Kwon, *Adv. Opt. Mater.* **2018**, *6*, 1701258.
[25] J. A. Lee, W. T. Kim, M. Jazbinsek, D. Kim, S. H. Lee, S. H. Lee, I. C. Yu, W. Yoon, H. Yun, F. Rotermund, O. P. Kwon, *Adv. Opt. Mater.* **2020**, *8*, 1901921.
[26] G. A. Valdivia-Berroeta, E. W. Jackson, K. C. Kenney, A. X. Wayment, I. C. Tangen, C. B. Bahr, S. J. Smith, D. J. Michaelis, J. A. Johnson, *Adv. Funct. Mater.* **2020**, *30*, 1904786.
[27] I. Aramburu, J. Ortega, C. L. Folcia, J. Etxebarria, *Appl. Phys. Lett.* **2014**, *104*, 071107.
[28] S. K. Kurtz, T. T. Perry, *J. Appl. Phys.* **1968**, *39*, 3798.
[29] C. U. Jeong, B. J. Kang, S. H. Lee, S. C. Lee, W. T. Kim, M. Jazbinsek, W. Yoon, H. Yun, D. Kim, F. Rotermund, O. P. Kwon, *Adv. Funct. Mater.* **2018**, *28*, 1801143.
[30] J. H. Seok, U. Puc, S. J. Kim, W. J. Yoon, H. S. Yun, I. C. Yu, F. Rotermund, D. W. Kim, M. Jazbinsek, O. P. Kwon, *Adv. Opt. Mater.* **2021**, *9*, 2100618.
[31] G. E. Yoon, J. H. Seok, U. Puc, B. R. Shin, W. J. Yoon, H. S. Yun, D. W. Kim, I. C. Yu, F. Rotermund, M. Jazbinsek, O. P. Kwon, *Adv. Sci.* **2022**, *9*, 2201391.
[32] A. Sher Gill, S. Kalainathan, *J. Phys. Chem. Solids* **2011**, *72*, 1002.
[33] Z. Yang, L. Mutter, M. Stillhart, B. Ruiz, S. Aravazhi, M. Jazbinsek, A. Schneider, V. Gramlich, P. Günter, *Adv. Funct. Mater.* **2007**, *17*, 2018.
[34] B. Ruiz, Z. Yang, V. Gramlich, M. Jazbinsek, P. Günter, *J. Mater. Chem.* **2006**, *16*, 2839.
[35] Z. Sun, X. Liu, X. Wang, L. Li, X. Shi, S. Li, C. Ji, J. Luo, M. Hong, *Cryst. Growth Des.* **2012**, *12*, 6181.
[36] G. A. Valdivia-Berroeta, L. K. Heki, E. A. McMurray, L. A. Foote, S. H. Nazari, L. Y. Serafin, S. J. Smith, D. J. Michaelis, J. A. Johnson, *Adv. Opt. Mater.* **2018**, *6*, 1800383.
[37] G. A. Valdivia-Berroeta, K. C. Kenney, E. W. Jackson, J. C. Bloxham, A. X. Wayment, D. J. Brock, S. J. Smith, J. A. Johnson, D. J. Michaelis, *J. Mater. Chem. C* **2020**, *8*, 11079.
[38] P. J. Kim, J. H. Jeong, M. Jazbinsek, S. B. Choi, I. H. Baek, J. T. Kim, F. Rotermund, H. Yun, Y. S. Lee, P. Günter, O. P. Kwon, *Adv. Funct. Mater.* **2012**, *22*, 200.
[39] J. H. Jeong, B. J. Kang, J. S. Kim, M. Jazbinsek, S. H. Lee, S. C. Lee, I. H. Baek, H. Yun, J. Kim, Y. S. Lee, J. H. Lee, J. H. Kim, F. Rotermund, O. P. Kwon, *Sci. Rep.* **2013**, *3*, 3200.
[40] S. H. Lee, B. J. Kang, B. W. Yoo, S. C. Lee, S. J. Lee, M. Jazbinsek, H. Yun, F. Rotermund, O. P. Kwon, *Adv. Funct. Mater.* **2017**, *27*, 1605583.
[41] S. I. Kim, B. J. Kang, C. U. Jeong, M. H. Shin, W. T. Kim, M. Jazbinsek, W. Yoon, H. Yun, D. Kim, F. Rotermund, O. P. Kwon, *Adv. Opt. Mater.* **2019**, *7*, 1801495.
[42] S. I. Kim, W. T. Kim, J. H. Seok, M. Jazbinsek, W. Yoon, I. C. Yu, H. Yun, D. Kim, F. Rotermund, O. P. Kwon, *Adv. Opt. Mater.* **2020**, *8*, 1901840.
[43] S. H. Lee, B. J. Kang, J. S. Kim, B. W. Yoo, J. H. Jeong, K. H. Lee, M. Jazbinsek, J. W. Kim, H. Yun, J. Kim, Y. S. Lee, F. Rotermund, O. P. Kwon, *Adv. Opt. Mater.* **2015**, *3*, 756.
[44] S. J. Lee, B. J. Kang, M. H. Shin, S. C. Lee, S. H. Lee, M. Jazbinsek, H. Yun, D. Kim, F. Rotermund, O. P. Kwon, *Adv. Opt. Mater.* **2018**, *6*, 1700930.
[45] S. C. Lee, B. J. Kang, M. J. Koo, S. H. Lee, J. H. Han, J. Y. Choi, W. T. Kim, M. Jazbinsek, H. Yun, D. Kim, F. Rotermund, O. P. Kwon, *Adv. Opt. Mater.* **2017**, *5*, 1600758.
[46] M. H. Shin, W. T. Kim, S. I. Kim, S. H. Lee, I. C. Yu, M. Jazbinsek, W. Yoon, H. Yun, D. Kim, F. Rotermund, O. P. Kwon, *Adv. Opt. Mater.* **2019**, *7*, 1900953.
[47] J. Y. Choi, S. J. Lee, S. C. Lee, C. U. Jeong, M. Jazbinsek, H. Yun, B. J. Kang, F. Rotermund, O. P. Kwon, *J. Mater. Chem. C* **2017**, *5*, 12602.
[48] S. H. Lee, J. Lu, S. J. Lee, J. H. Han, C. U. Jeong, S. C. Lee, X. Li, M. Jazbinsek, W. Yoon, H. Yun, B. J. Kang, F. Rotermund, K. A. Nelson, O. P. Kwon, *Adv. Mater.* **2017**, *29*, 1701748.
[49] M. H. Shin, W. T. Kim, S. I. Kim, S. J. Kim, I. C. Yu, S. W. Kim, M. Jazbinsek, W. Yoon, H. Yun, F. Rotermund, O. P. Kwon, *Adv. Sci.* **2020**, *7*, 2001738.
[50] D. Kim, W. T. Kim, J. H. Han, J. A. Lee, S. H. Lee, B. J. Kang, M. Jazbinsek, W. Yoon, H. Yun, D. Kim, S. Bezouw, J. Campo, W. Wenseleers, F. Rotermund, O. P. Kwon, *Adv. Opt. Mater.* **2020**, *8*, 1902099.
[51] J. Shi, Y. He, F. Liang, X. Zhang, D. Xu, J. Yao, G. Zhang, Z. Hu, J. Yao, Y. Wu, *J. Mater. Chem. C* **2020**, *8*, 4226.
[52] D. Kim, W. T. Kim, J. H. Seok, I. C. Yu, M. Jazbinsek, W. Yoon, H. Yun, D. Kim, F. Rotermund, O. P. Kwon, *J. Mater. Chem. C* **2020**, *8*, 10078.
[53] M. A. Spackman, J. J. McKinnon, *CrystEngComm* **2002**, *4*, 378.
[54] M. A. Spackman, D. Jayatilaka, *CrystEngComm* **2009**, *11*, 19.
[55] J. J. McKinnon, D. Jayatilaka, M. A. Spackman, *Chem. Commun.* **2007**, *37*, 3814.
[56] S. H. Lee, M. Jazbinsek, C. P. Hauri, O. P. Kwon, *CrystEngComm* **2016**, *18*, 7180.
[57] J. Kim, Y. C. Park, J. H. Seok, M. Jazbinsek, O. P. Kwon, *Adv. Opt. Mater.* **2021**, *9*, 2001521.
[58] O. P. Kwon, S. J. Kwon, H. Figi, M. Jazbinsek, P. Gunter, *Adv. Mater.* **2008**, *20*, 543.
[59] A. Choubey, O. P. Kwon, M. Jazbinsek, P. Gunter, *Cryst. Growth Des.* **2007**, *7*, 402.
[60] J. Shi, F. Liang, Y. He, X. Zhang, Z. Lin, D. Xu, Z. Hu, J. Yao, Y. Wu, *Chem. Commun.* **2019**, *55*, 7950.
[61] W. Zhang, Z. Wang, X. Zhang, Y. Wang, D. Xu, Z. Hu, J. Yao, Y. Wu, *Cryst. Growth Des.* **2022**, *22*, 3311.